

# Two Distinct Thermodynamic Gradients for Cellular Metalation of Vitamin B<sub>12</sub>

Tessa R. Young,\* Evelyne Deery, Andrew W. Foster, Maria Alessandra Martini, Deenah Osman, Martin J. Warren, and Nigel J. Robinson\*



Cite This: <https://doi.org/10.1021/jacsau.3c00119>



Read Online

ACCESS |



Metrics & More



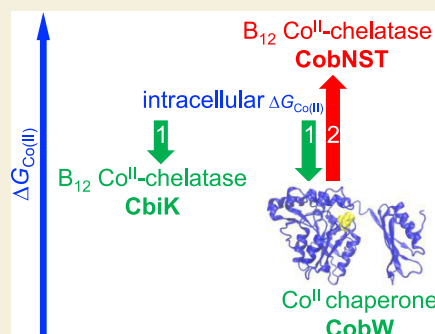
Article Recommendations



Supporting Information

**ABSTRACT:** The acquisition of Co<sup>II</sup> by the corrin component of vitamin B<sub>12</sub> follows one of two distinct pathways, referred to as early or late Co<sup>II</sup> insertion. The late insertion pathway exploits a Co<sup>II</sup> metallochaperone (CobW) from the COG0523 family of G3E GTPases, while the early insertion pathway does not. This provides an opportunity to contrast the thermodynamics of metalation in a metallochaperone-requiring and a metallochaperone-independent pathway. In the metallochaperone-independent route, sirohydrochlorin (SHC) associates with the CbiK chelatase to form Co<sup>II</sup>-SHC. Co<sup>II</sup>-buffered enzymatic assays indicate that SHC binding enhances the thermodynamic gradient for Co<sup>II</sup> transfer from the cytosol to CbiK. In the metallochaperone-dependent pathway, hydrogenobyrinic acid *a,c*-diamide (HBAD) associates with the CobNST chelatase to form Co<sup>II</sup>-HBAD. Here, Co<sup>II</sup>-buffered enzymatic assays indicate that Co<sup>II</sup> transfer from the cytosol to HBAD-CobNST must somehow traverse a highly unfavorable thermodynamic gradient for Co<sup>II</sup> binding. Notably, there is a favorable gradient for Co<sup>II</sup> transfer from the cytosol to the Mg<sup>II</sup>GTP-CobW metallochaperone, but further transfer of Co<sup>II</sup> from the GTP-bound metallochaperone to the HBAD-CobNST chelatase complex is thermodynamically unfavorable. However, after nucleotide hydrolysis, Co<sup>II</sup> transfer from the chaperone to the chelatase complex is calculated to become favorable. These data reveal that the CobW metallochaperone can overcome an unfavorable thermodynamic gradient for Co<sup>II</sup> transfer from the cytosol to the chelatase by coupling this process to GTP hydrolysis.

**KEYWORDS:** bioinorganic chemistry, metalation, metalloprotein, chelatase, metallochaperone, GTPase, vitamin B<sub>12</sub>



## INTRODUCTION

Most metalloenzymes (~70%) are thought to acquire metal ions directly from nonspecific exchangeable sites inside cells with a further 25% containing preassembled metal cofactors.<sup>1</sup> Cofactors such as heme, cofactor F<sub>430</sub>, chlorophyll, and vitamin B<sub>12</sub> acquire Fe<sup>II</sup>, Ni<sup>II</sup>, Mg<sup>II</sup>, and Co<sup>II</sup> from chelataes.<sup>2,3</sup> Some chelataes such as CbiK for vitamin B<sub>12</sub> biosynthesis are thought to directly acquire metal (Co<sup>II</sup>) from the exchangeable cytosolic sites, while others such as CobNST from the alternative vitamin B<sub>12</sub> biosynthesis pathway acquire metal (Co<sup>II</sup>) from specific metallochaperones (in this case, CobW), which, in turn, acquire metal from the exchangeable sites.<sup>4</sup> How is Co<sup>II</sup> driven from nonspecific intracellular exchangeable sites to vitamin B<sub>12</sub> either via a chelatae alone (CbiK) or via a chelatae and a metallochaperone (CobNST and CobW)?<sup>5</sup>

CbiK inserts Co<sup>II</sup> into the substrate sirohydrochlorin (SHC) at an early stage (before ring contraction) in the vitamin B<sub>12</sub> synthesis pathway first discovered in anaerobic bacteria (Figure 1a).<sup>6</sup> CbiK is a relatively small protein (~29 kDa in *Salmonella enterica* serovar Typhimurium strain 1344, referred to as *Salmonella* hereafter) that works without accessory proteins or nucleotide cofactors.<sup>7</sup> In the alternative (aerobic) pathway, Co<sup>II</sup> is inserted at a late stage into the ring-contracted vitamin

B<sub>12</sub> precursor hydrogenobyrinic acid *a,c*-diamide (HBAD) by the multicomponent chelatae CobNST (13 subunits), which, in common with the structurally related magnesium chelatae for chlorophyll biosynthesis,<sup>8</sup> couples metal insertion with the hydrolysis of ATP (Figure 1a).<sup>9,10</sup> The additional chaperone (CobW) is, for some reason, also used to supply Co<sup>II</sup> to CobNST *in vivo*.<sup>4</sup>

Vitamin B<sub>12</sub> is an essential dietary component but absent in plants. Supplements are therefore recommended for vegans. While the complete chemical synthesis of vitamin B<sub>12</sub> has been achieved, these elaborate natural product syntheses are unsuitable for commercial-scale production.<sup>11,12</sup> Instead, vitamin B<sub>12</sub> is manufactured exclusively through bioprocessing. However, the synthesis of vitamin B<sub>12</sub> is restricted to a subset of bacteria and archaea, which does not include organisms such as *Escherichia coli* that are commonly used in manufacturing.

**Received:** March 14, 2023

**Revised:** April 13, 2023

**Accepted:** April 25, 2023

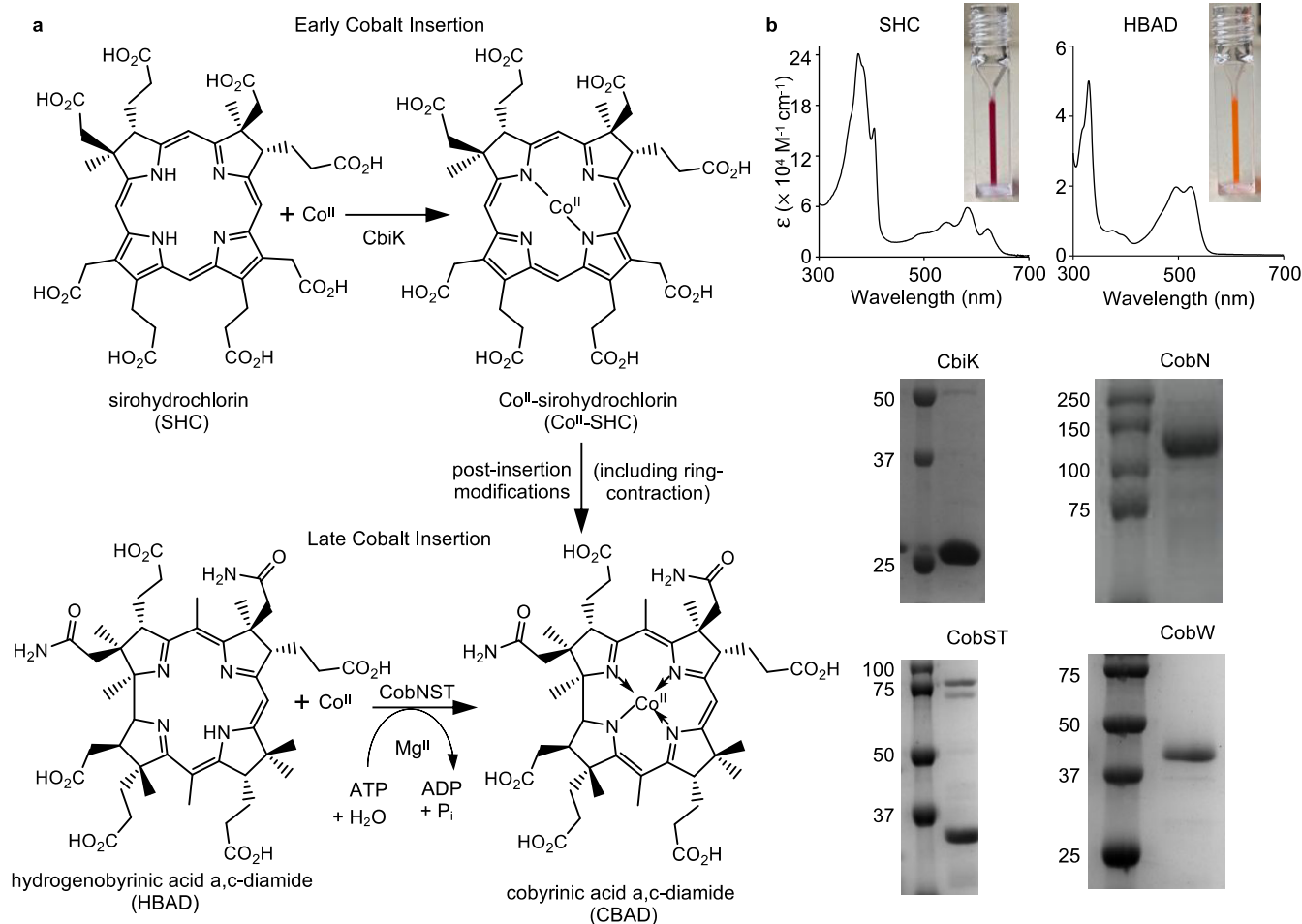


**Figure 1.** Enzyme-catalyzed cobalt insertion reactions for the biosynthesis of vitamin B<sub>12</sub>. (a) The two biosynthetic pathways for vitamin B<sub>12</sub> involve early- and late-stage insertion of the catalytic cobalt ion, respectively.<sup>2,7</sup> Co<sup>II</sup> insertion into the porphyrin substrate sirohydrochlorin (SHC) to form cobalt-sirohydrochlorin (Co<sup>II</sup>-SHC) is catalyzed by the cobaltochelatase CbiK.<sup>17</sup> Co<sup>II</sup> insertion into the ring-contracted substrate hydrogenobyric acid a,c-diamide (HBAD) to form cobyrinic acid a,c-diamide (CBAD) is catalyzed by the cobaltochelatase CobNST, which requires energy input from ATP hydrolysis and an additional metallochaperone (CobW) for Co<sup>II</sup> supply *in vivo*.<sup>4,9</sup> (b) Absorbance spectra of isolated substrates and SDS-PAGE analyses of isolated enzymes (full-length gel images shown in Figure S1).

When the biosynthetic pathway involving CobW and CobNST was introduced into *E. coli*, B<sub>12</sub> production stalled at the point of Co<sup>II</sup> insertion in standard culture media.<sup>4</sup> Intriguingly, the F<sub>430</sub> pathway from methanobacteria introduced into *E. coli* also stalled at the point of metal (Ni<sup>II</sup>) insertion even in Ni<sup>II</sup>-supplemented media, and this was overcome by introducing genes encoding an additional Ni<sup>II</sup> importer.<sup>13</sup> These observations suggest that exchangeable metals could be maintained at different availabilities in different organisms leading to mismatches between heterologously introduced proteins and host cells such as *E. coli*. An understanding of the thermodynamic gradients that supply metals to proteins and cofactors in a cellular context is needed to enable optimization and exploitation of metalloproteins in engineering biology.

Intracellular metal availabilities have been estimated as free energies for forming metal complexes, by calibrating the responses of bacterial metal sensing transcriptional regulators.<sup>14</sup> The thermodynamic gradient from exchangeable intracellular sites to CbiK (based on the *K<sub>D</sub>* of *Salmonella* CbiK for Co<sup>II</sup>) was calculated to result in 15% metalation of CbiK with Co<sup>II</sup> (the predominant metal) in a so-called “idealized” cell, where the Co<sup>II</sup> sensor (RcnR) is at the midpoint of its response range.<sup>14</sup> In *E. coli* grown in LB media,

aerobically or anaerobically, RcnR is well below the midpoint of its Co<sup>II</sup>-sensing range, which would give negligible metalation of CbiK in *E. coli*, suggesting that this may also be true in *Salmonella*.<sup>15</sup> However, the *K<sub>D</sub>* for Co<sup>II</sup> of CbiK was measured in the absence of its substrate sirohydrochlorin (SHC) and notably for the related chelatase for cofactor F<sub>430</sub>, CfbA, metal (Ni<sup>II</sup>) is partly ligated to SHC in an intermediate complex.<sup>16</sup> Here, we have examined Co<sup>II</sup> acquisition by CbiK in a metal-buffered *in vitro* enzymatic assay to account for such substrate binding. Co<sup>II</sup> insertion by CobNST (from *Rhodobacter capsulatus*) has also been reconstituted in a metal-buffered *in vitro* enzymatic assay. The thermodynamic gradients for the flow of Co<sup>II</sup> in the two biosynthetic pathways for vitamin B<sub>12</sub> have thus been defined, discovering that the two chelatases require substantially (almost two orders of magnitude) different Co<sup>II</sup> availabilities and uncovering the mechanistic requirement for an additional metallochaperone (CobW) in the CobNST pathway.

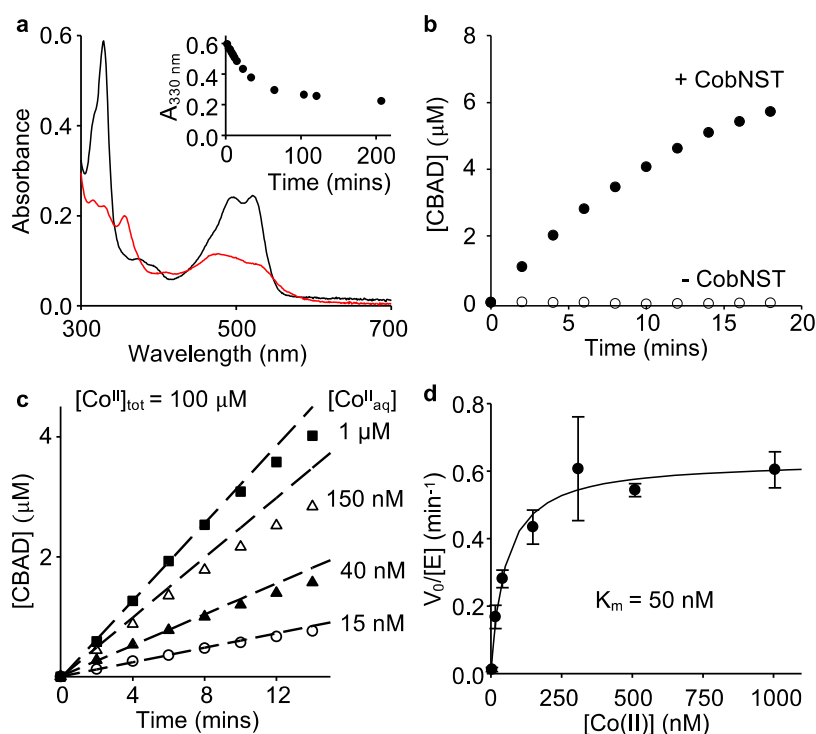


**Figure 2.** Buffere metal concentration-dependent rate of conversion of HBAD to CBAD by CobNST via steady-state kinetics. (a) UV–visible absorbance of HBAD (11.6  $\mu\text{M}$ ) before (black line) and 3.5 h after (red line) incubation with  $\text{Co}^{\text{II}}$  (100  $\mu\text{M}$ ) and CobNST (3  $\mu\text{M}$  of each subunit) in the presence of  $\text{MgCl}_2$  (10 mM) and ATP (5 mM). The inset shows absorbance at 330 nm over time, following the addition of cobalt. (b) Initial formation of CBAD when HBAD (10  $\mu\text{M}$ ) was incubated with  $\text{Co}^{\text{II}}$  (100  $\mu\text{M}$ ),  $\text{Mg}^{\text{II}}$  (10 mM), and ATP (5 mM) in the presence (filled circles) or absence (open circles) of CobNST (3  $\mu\text{M}$  of each subunit). (c) CobNST-catalyzed metalation of HBAD (initial concentration 10  $\mu\text{M}$ ) when available  $[\text{Co}^{\text{II}}_{\text{aq}}]$  was buffered to different availabilities using L-histidine to achieve sub-micromolar concentrations (Table S1). Initial rates ( $v_0$ ) were calculated from linear fits of the data for the first 6 min of reaction at each condition (shown by dashed lines). (d) Steady-state kinetics for  $\text{Co}^{\text{II}}$  insertion into HBAD by CobNST. Initial rates of metalation ( $v_0$ ) relative to enzyme concentration ( $[\text{E}]_{\text{tot}} = 0.5 \mu\text{M}$ ) were determined at varying available  $[\text{Co}^{\text{II}}]$  (see Table S1 for experimental conditions). Data are the mean  $\pm$  s.d. of three independent experiments. All reactions were carried out in 50 mM Hepes buffer pH 7.0, 100 mM NaCl.

## RESULTS

### Production of Reagents for Enzymatic Assays

Substrates, sirohydrochlorin (SHC) and hydrogenobyrrinic acid *a,c*-diamide (HBAD) were synthesized *in vitro* and *in vivo*, respectively (Figure 1b). SHC was synthesized from *S*-adenosyl-L-methionine and aminolevulinic acid using copurified enzymes recovered from *E. coli* expressing tagged version of enzymes HemB and SirC from *Methanothermobacter thermautotrophicus*, HemC and HemD from *Bacillus megaterium*, and CobA from *Methanosarcina barkeri*.<sup>18</sup> HBAD was isolated from *E. coli* engineered to contain the set of genes (*cobAIGJFMKLHB*) for its biosynthesis.<sup>19</sup> Diagnostic UV–visible absorbance spectra were recorded for both substrates (Figure 1b). The chelases, CbiK from *Salmonella* and CobNST from *R. capsulatus*, were overexpressed and purified from *E. coli*: CbiK and CobN individually and CobST coexpressed and isolated as a complex (Figures 1b, S1 and refs 14, 20). Metallochaperone CobW from *R. capsulatus* was overexpressed and purified from *E. coli* (Figures 1b, S1 and ref 4).

### CobNST Metalates HBAD at Nanomolar $\text{Co}^{\text{II}}$ Concentrations

The cobalt-concentration dependence of CobNST chelase activity was determined by reconstituting the metalation reaction *in vitro*. Metalation of HBAD to form cobyrinic acid *a,c*-diamide (CBAD) was followed by changes in the UV–

visible absorbance of the tetrapyrrole (Figure 2a), as previously reported.<sup>9,10</sup> An extinction coefficient correlating absorbance change to conversion of HBAD to CBAD was determined ( $\Delta\epsilon_{330\text{ nm}} = -3.0 \times 10^4 \text{ M}^{-1} \text{ cm}^{-1}$ ; Figures 2a and S2). Chemical insertion of  $\text{Co}^{\text{II}}$  into HBAD was not detected in the absence of the CobNST enzyme (Figure 2b), and the rate of reaction increased proportionally with CobNST concentration, allowing reliable estimation of enzyme activity under the experimental conditions (Figure S3). To reflect intracellular metalation, avoiding artificially limiting the reaction due to the total amount of metal, available  $\text{Co}^{\text{II}}$  concentrations were controlled using ligands histidine (His) or ethyleneglycol-bis( $\beta$ -aminoethyl ether)-*N,N',N',N'*-tetraacetic acid (EGTA) to buffer  $[\text{Co}^{\text{II}}_{\text{aq}}]$  from micromolar to nanomolar availabilities while retaining an excess of total  $[\text{Co}^{\text{II}}]$  in each reaction mixture (Table S1). At sub-micromolar buffered  $\text{Co}^{\text{II}}$  concentrations, the enzyme-catalyzed reaction slowed significantly (Figure 2c, Table S1), following Michaelis–Menten kinetics with a fitted  $k_{\text{cat}}$  of  $0.63 \text{ min}^{-1}$  for metal chelation (Figure 2d), noting that similarly slow *in vitro* reaction kinetics have been estimated for the related magnesium chelase from *Synechocystis*.<sup>21</sup> Importantly, the fitted  $K_{\text{m}}$  for  $\text{Co}^{\text{II}}$  of HBAD–CobNST is 50 nM (Figure 2d).

### $\text{Co}^{\text{II}}$ Partitioning between CobW and CobNST

The measured  $K_{\text{m}}$  for  $\text{Co}^{\text{II}}$  suggests that CobNST will not be metalated at buffered intracellular  $\text{Co}^{\text{II}}$  availabilities, previously estimated as picomolar to low nanomolar concentrations in *E.*

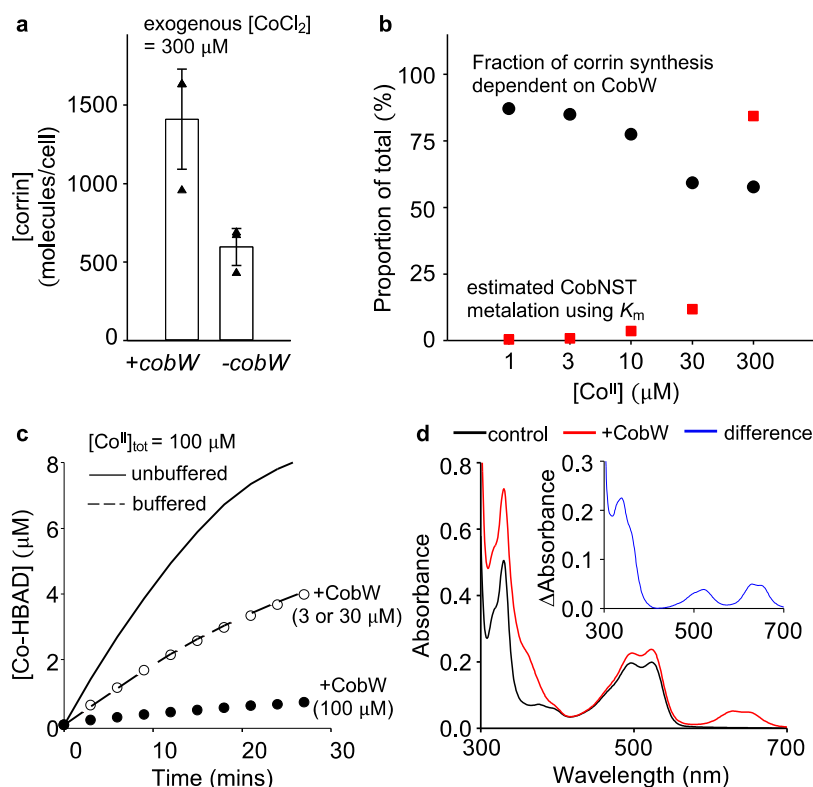


**Figure 3.** CobW enhances corrin biosynthesis *in vivo*, but  $\text{Mg}^{\text{II}}$ -GTP-CobW quenches the formation of CBAD by CobNST *in vitro*. (a) Corrin production by engineered *E. coli*\* strains with and without *cobW* following 4 h exposure to  $300 \mu\text{M}$   $\text{CoCl}_2$ . Data are the mean  $\pm$  s.d. of three biologically independent replicates. Triangle shapes represent individual experiments. (b) All data refer to *E. coli*\* cells grown in LB media with 1– $300 \mu\text{M}$   $\text{CoCl}_2$  supplementation. CobW-dependent corrin synthesis was determined from the difference in measured corrin production for +cobW versus –cobW *E. coli*\* strains as a proportion of total corrin produced by the +cobW strain (panel (a) and ref 4). CobNST metalation was estimated using  $K_m$  for  $\text{Co}^{\text{II}}$  and measured intracellular  $\text{Co}^{\text{II}}$  availabilities in *E. coli*\* at each growth condition (Figure 2d, Table S2 and ref 4). (c) CobNST-catalyzed formation of CBAD when  $\text{Co}^{\text{II}}$  ( $100 \mu\text{M}$ ) was supplied in the presence of a metal buffering ligand (6 mM L-His;  $[\text{Co}_{\text{aq}}^{\text{II}}] = 40 \text{ nM}$ ) without CobW (dashed line), with 3 or  $30 \mu\text{M}$  CobW (open circles, indistinguishable) or with  $100 \mu\text{M}$  CobW (closed circles). The solid line shows control experiment when  $\text{Co}^{\text{II}}$  was supplied in the absence of a buffering ligand. (d) Initial absorbance spectra of reactions from (c) without CobW (black trace) or with  $100 \mu\text{M}$  CobW (red trace). Difference spectra (inset) matches the known absorbance spectrum of  $\text{Co}^{\text{II}}$  $\text{Mg}^{\text{II}}$ -GTP-CobW with a concentration of  $81 \mu\text{M}$  inferred from signal intensity at  $339 \text{ nm}$ .<sup>†</sup> All reactions were performed in 50 mM Hepes pH 7.0, 100 mM NaCl with  $\text{Mg}^{\text{II}}$  (10 mM), ATP (5 mM), GTP (1 mM), and CobNST (3  $\mu\text{M}$  of each subunit).

*coli* and *Salmonella*<sup>4,14,15</sup> (Table S2). Vitamin  $\text{B}_{12}$  biosynthesis was previously shown to be substantially dependent upon CobW in cultures of *E. coli* engineered to synthesize  $\text{B}_{12}$  (denoted *E. coli*\*), grown in LB media containing up to  $30 \mu\text{M}$   $\text{Co}^{\text{II}}$  (ref 4). Consistent with these observations, using  $K_m$   $\text{Co}^{\text{II}}$  for CobNST, now predicts only 12% metalation of CobNST in the absence of CobW at  $30 \mu\text{M}$   $\text{Co}^{\text{II}}$  (Table S2). Cells exposed to  $300 \mu\text{M}$   $\text{Co}^{\text{II}}$  showed maximum de-repression of the *E. coli*  $\text{Co}^{\text{II}}$  sensor RcnR, which was previously used in calibrations to determine the intracellular free energies of available  $\text{Co}^{\text{II}}$  in cells grown up to  $30 \mu\text{M}$   $\text{Co}^{\text{II}}$ . Figure 3a now shows CobW-dependent and CobW-independent  $\text{B}_{12}$  synthesis in cells grown in  $300 \mu\text{M}$   $\text{Co}^{\text{II}}$ , revealing substantial CobW-independent synthesis at this highly elevated  $[\text{Co}^{\text{II}}]$  consistent with an estimated 84% metalation of CobNST using the newly determined  $K_m$   $\text{Co}^{\text{II}}$  (Figure 3b and Table S2). It is anticipated that the function of CobW is to make  $\text{Co}^{\text{II}}$  available to the CobNST chelatase at lower and more typical  $\text{Co}^{\text{II}}$  levels.

Intriguingly, we do still observe some ( $\sim 2$ -fold) CobW-dependent  $\text{B}_{12}$  synthesis even in cultures grown in LB media containing  $300 \mu\text{M}$   $\text{Co}^{\text{II}}$  where CobNST is calculated to be largely capable of independent metalation (Figure 3a,b).

To investigate the transfer of  $\text{Co}^{\text{II}}$  between the metallochaperone and chelatase *in vitro*, CobNST chelatase activity

was measured at a range of available  $[\text{Co}^{\text{II}}]$  (with total mol of  $\text{Co}^{\text{II}}$  in excess relative to total mol CobW), in the absence and presence of CobW, to discover whether CobW can restore enzyme activity at limiting  $[\text{Co}^{\text{II}}]$  availabilities (Figure S4). Surprisingly, CobW (in the presence of its prerequisite cofactor  $\text{Mg}^{\text{II}}$ -GTP) had no observable effect on reaction rates when supplied in 5-fold excess of the chelatase subunits. Importantly, Figure 3c shows that, when supplied at an equimolar amount to the total amount of  $\text{Co}^{\text{II}}$ , CobW quenched the chelatase activity. At such high  $[\text{CobW}]$ , the absorbance spectra revealed significant changes and the difference spectra are consistent with the known spectral features of  $\text{Co}^{\text{II}}$  $\text{Mg}^{\text{II}}$ -GTP-CobW (Figure 3d). The increased absorbance at  $339 \text{ nm}$ , resulting from ligand to metal charge transfer (LMCT) between sulfur donors of CobW and the ligated  $\text{Co}^{\text{II}}$  ion ( $\epsilon_{339 \text{ nm}} = 2800 \text{ M}^{-1} \text{ cm}^{-1}$  ref 4), indicates sequestration of most (81%) of the  $\text{Co}^{\text{II}}$  in the assay. An excess concentration of CobW (in relation to  $\text{Co}^{\text{II}}$ ) was sufficient to sequester all  $\text{Co}^{\text{II}}$  in the assay and fully quench the enzyme activity of CobNST (Figure S5). These data indicate that the GTP-bound form of CobW acquired  $\text{Co}^{\text{II}}$  from the reaction solution and, due to its high affinity ( $\text{Mg}^{\text{II}}$ -GTP-CobW  $K_{\text{Co}(\text{II})} = 30 \text{ pM}^*$ ), withheld metal from the chelatase inhibiting the metal insertion reaction. GTP hydrolysis weakens CobW



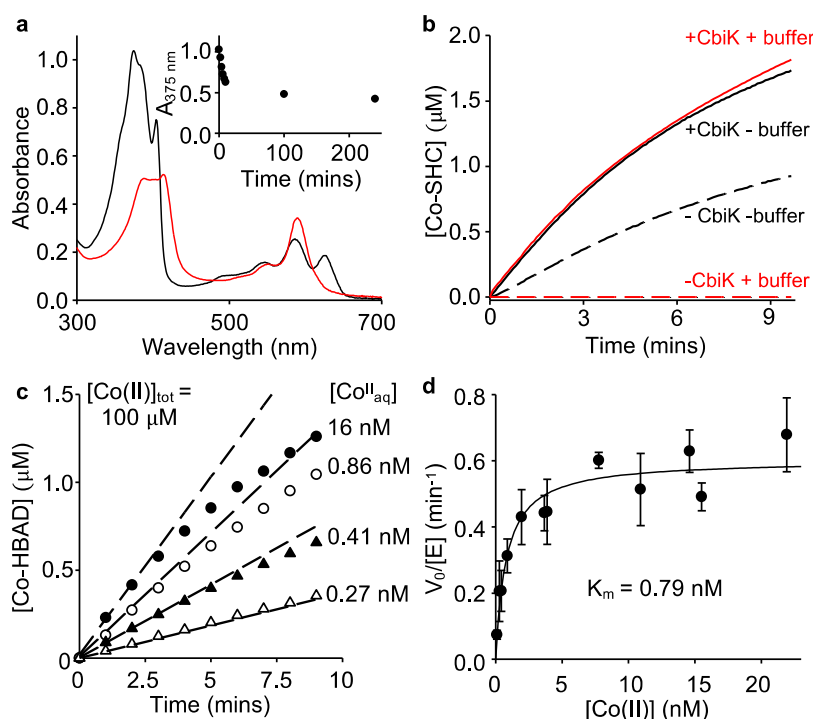


**Figure 4.** Buffered metal concentration-dependent rate of conversion of SHC to  $\text{Co}^{\text{II}}$ -SHC by CbiK via steady-state kinetics. (a) UV–visible absorbance of SHC ( $4.3 \mu\text{M}$ ) before (black line) and 4 h after (red line) incubation with  $\text{Co}^{\text{II}}$  ( $100 \mu\text{M}$ ) and CbiK ( $0.5 \mu\text{M}$ ) in the presence of His ( $1 \text{ mM}$ ). (b) Formation of Co-SHC when SHC ( $5 \mu\text{M}$ ) was incubated with  $\text{Co}^{\text{II}}$  ( $100 \mu\text{M}$ ) in the presence (red lines) or absence (black lines) of a histidine metal buffer ( $1 \text{ mM}$ ) and CbiK ( $0.5 \mu\text{M}$ , as labeled). (c) CbiK-catalyzed metalation of SHC (initial concentration  $5 \mu\text{M}$ ) when available  $[\text{Co}^{\text{II}}_{\text{aq}}]$  was buffered using NTA or EGTA to achieve sub-nanomolar concentrations (Table S3). Initial rates ( $v_0$ ) were calculated from linear fits of the data for the first 2 min of reaction at each condition (shown by dashed lines). (d) Steady-state kinetics for  $\text{Co}^{\text{II}}$  insertion into SHC by CbiK. Initial rates of metalation ( $v_0$ ) relative to enzyme concentration ( $[\text{E}]_{\text{tot}} = 0.375 \mu\text{M}$ ) were determined at varying available  $[\text{Co}^{\text{II}}]$  (see Table S3 for experimental conditions). Data are the mean  $\pm$  s.d. of three independent experiments. All reactions were carried out in  $50 \text{ mM}$  Hepes buffer pH  $7.0$ ,  $100 \text{ mM}$  NaCl.

affinity for  $\text{Co}^{\text{II}}$  ( $\text{Mg}^{\text{II}}\text{GDP-CobW } K_{\text{Co}(\text{II})} = 100 \text{ nM}^4$ ), which should enable transfer to CobNST, implying that hydrolysis did not occur under the *in vitro* reaction conditions. Moreover, addition of GDP to the reaction mixture did not activate the chelatase reaction (Figure S4b). A GTPase-activating protein (GAP) may be missing from the *in vitro* reaction, and in direct competition,  $\text{Mg}^{\text{II}}\text{GTP-CobW}$  acquires  $\text{Co}^{\text{II}}$ , whereas CobNST does not as predicted from  $K_{\text{D}}$  versus  $K_{\text{m}}$ .

#### CbiK Metalates SHC at Sub-Nanomolar $\text{Co}^{\text{II}}$ Concentrations

The  $\text{Co}^{\text{II}}$  concentration dependence of the CbiK chelatase activity from the early insertion pathway was previously explored based on the  $K_{\text{D}}$  of CbiK alone.<sup>14</sup> To investigate whether the presence of the substrate, SHC, may enhance  $\text{Co}^{\text{II}}$  acquisition by CbiK from the intracellular milieu, metalation reactions were reconstituted *in vitro* using defined  $\text{Co}^{\text{II}}$ -buffers.  $\text{Co}^{\text{II}}$  insertion into SHC was followed via changes in the UV–visible absorbance of the tetrapyrrole (Figure 4a), as previously reported.<sup>22</sup> An extinction coefficient correlating absorbance change with conversion of SHC to  $\text{Co}^{\text{II}}$ -SHC was determined to be  $\Delta\epsilon_{330 \text{ nm}} = -1.4 \times 10^5 \text{ M}^{-1} \text{ cm}^{-1}$  (Figures 4a, S2). At excess unbuffered  $\text{Co}^{\text{II}}$  concentrations, chemical (nonenzymatic) metalation of SHC was observed, but buffering of  $\text{Co}^{\text{II}}$  to sub-micromolar availabilities prevented the nonenzymatic reaction (Figure 4b). At such buffered metal availabilities, the rate of reaction increased proportionally with CbiK concentration (within an identified set of experimental conditions, Figure S3), allowing reliable estimation of enzyme activity.

Available  $\text{Co}^{\text{II}}$  concentrations were controlled using His or EGTA to buffer  $[\text{Co}^{\text{II}}_{\text{aq}}]$  from nanomolar to picomolar availabilities while retaining an excess of total  $[\text{Co}^{\text{II}}]$  in each reaction mixture (Figure 4c, Table S3). The enzyme-catalyzed reaction followed Michaelis–Menten kinetics with a fitted  $v_{\text{max}}$  of  $0.60 \text{ min}^{-1}$  and importantly a fitted  $K_{\text{m}}$  for  $\text{Co}^{\text{II}}$  of  $0.79 \text{ nM}$  (Figure 4d), in contrast to a  $K_{\text{D}}$  of  $14 \text{ nM}$  for CbiK alone.<sup>14</sup>

#### Responses of the *Salmonella* Sensor RcnR Used to Determine the Free Energies of Available Cobalt *In Vivo*

The  $>10$ -fold tighter  $K_{\text{m}}$  (relative to  $K_{\text{D}}$  of CbiK alone) increases estimated acquisition of  $\text{Co}^{\text{II}}$  in a cell (Figure 4d, Table S2). However, metalation is still predicted to be low in an *E. coli* cytosol (grown in LB medium, Table S2) in the absence of metal supplementation where  $\text{Co}^{\text{II}}$  availability is substantially lower than idealized *Salmonella*.<sup>4</sup> Notably, *E. coli* does not normally make  $\text{B}_{12}$  and lacks a dedicated  $\text{Co}^{\text{II}}$  uptake system.<sup>23</sup> The CbiK protein used herein originates from *Salmonella*, an organism which makes  $\text{B}_{12}$  under anaerobic growth conditions. To estimate the metalation state of the chelatase in its native host,  $\text{Co}^{\text{II}}$  availability was measured in anaerobic *Salmonella* confirmed to be producing vitamin  $\text{B}_{12}$  (Figure S6). Cultures were grown in LB media containing varied levels of exogenous metal (by supplementing media with either  $\text{CoCl}_2$  or EDTA) to elicit responses from the *Salmonella*  $\text{Co}^{\text{II}}$  sensor RcnR. Changes in the abundance of the RcnR-regulated *rcnA* transcripts in isolated RNA were monitored by qPCR (Figure 5a). Cellular  $\text{Co}^{\text{II}}$  availabilities under each growth condition were determined by calibrating

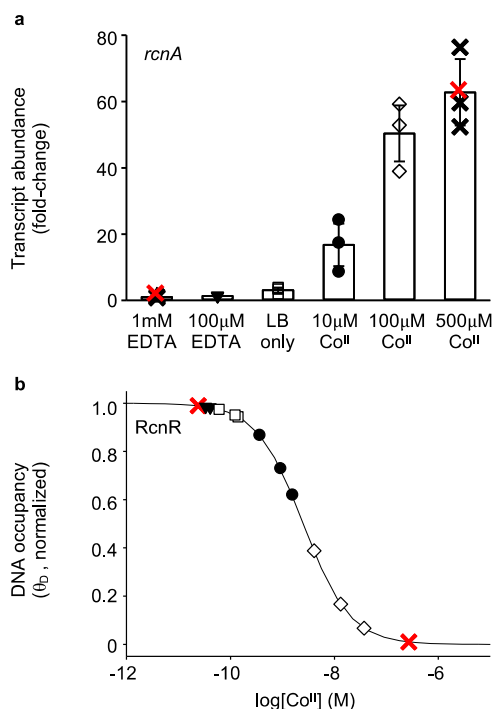


**Figure 5.** Intracellular  $\text{Co}^{\text{II}}$  availability in *Salmonella* under anaerobic conditions. (a) Abundance of *rcnA* transcripts (regulated by  $\text{Co}^{\text{II}}$  sensor RcnR) in anaerobic *Salmonella* cultures grown in LB media, measured by qPCR. Transcript abundances are relative to the control condition (1 mM EDTA, assigned a value of 1). Data are the mean  $\pm$  s.d. of three biologically independent replicates. (b) Solid line shows the calculated relationship between intracellular available  $[\text{Co}^{\text{II}}]$  and DNA occupancy of the  $\text{Co}^{\text{II}}$  sensor RcnR in *Salmonella*.<sup>14</sup> Fold changes in *rcnA* gene expression (from panel (a)) were converted to DNA occupancies of RcnR to determine intracellular  $\text{Co}^{\text{II}}$  availabilities for each culture. Red crosses in panel (a) indicate the minimum and maximum observed fold changes in gene expression and defined the boundary conditions ( $\theta_D$  of 0.01 and 0.99) for the dynamic range of the sensor response in panel (b).

the responses of *Salmonella* RcnR (Figure 5b), using recently described procedures.<sup>15</sup> Because  $\text{Zn}^{\text{II}}$ -mismetallation of CobW had been predicted in *E. coli*,<sup>4</sup> analogous experiments also determined cellular  $\text{Zn}^{\text{II}}$  availabilities in *Salmonella*, indicating that mismetallation of CobW would similarly occur in this heterologous host, albeit to a slightly lesser extent (Figure S7 and Table S5). In *Salmonella* cultured under anaerobic conditions in standard LB media,  $\text{Co}^{\text{II}}$  is more available compared to that reported for aerobic *E. coli* (Table S2). Together, tighter  $\text{Co}^{\text{II}}$  binding ( $K_m$ ) of CbiK in the presence of SHC and increased  $\text{Co}^{\text{II}}$  availability in anaerobic *Salmonella* enables the chelatase to become metalated in native host cells (12% predicted) substantively more than might otherwise have been estimated (Table S2).

## DISCUSSION

Figure 6 depicts the free energies for forming  $\text{Co}^{\text{II}}$ -complexes with CobW (in  $\text{Mg}^{\text{II}}$ GTP and  $\text{Mg}^{\text{II}}$ GDP forms), CobNST (with HBAD), and CbiK (with SHC). For CbiK-SHC and CobNST-HBAD, values are free energies for forming hypothetical  $\text{Co}^{\text{II}}$ -complexes that would be 50% metalated at concentrations equating to the respective  $K_m$ . Since  $k_{\text{cat}}$  for both chelation reactions were slow ( $<1 \text{ min}^{-1}$ , Figures 2 and 4),  $K_m$  should approximate  $K_D$  for  $\text{Co}^{\text{II}}$  binding to CbiK-SHC

and CobNST-HBAD (see eq 2). The free energy gradient for  $\text{Co}^{\text{II}}$  transfer from the intracellular milieu appears to be favorable for CbiK-SHC but unfavorable for CobNST-HBAD. This highlights the need for an accessory protein to assist cobalt acquisition in the CobNST pathway. Moreover, while the free energy gradient is highly favorable for  $\text{Co}^{\text{II}}$  transfer to  $\text{Mg}^{\text{II}}$ GTP-CobW, importantly post-hydrolysis, the gradient becomes favorable for transfer from  $\text{Mg}^{\text{II}}$ GDP-CobW to CobNST-HBAD. Calculations of metal transfer to and from the intracellular milieu are independent of protein concentration since the available metal is buffered. In contrast, the formation of  $\text{Mg}^{\text{II}}$ GTP-CobW-CobNST-HBAD complexes would be influenced by relative protein abundances. Departure from a 1:1 (chaperone:chelate) stoichiometry, as well as variance in measured affinities ( $K_D$  or  $K_m$ ), could modify the magnitude of metal transfer above or below 59% currently predicted (Calculation S1). Intermediate  $\text{Co}^{\text{II}}$ -complexes at high free energy ( $\text{Co}^{\text{II}}$  $\text{Mg}^{\text{II}}$ GDP-CobW and  $\text{Co}^{\text{II}}$ -CobNST-HBAD) must somehow avoid transfer of  $\text{Co}^{\text{II}}$  back to the intracellular exchangeable buffering molecules (Figure 6). Insertion of  $\text{Co}^{\text{II}}$  into HBAD by CobNST is ATP-dependent, and  $\text{Co}^{\text{II}}$  becomes expeditiously trapped in the ring-contracted tetrapyrrole at this step in the biosynthetic pathway. Presumably, hydrolysis of  $\text{Co}^{\text{II}}$  $\text{Mg}^{\text{II}}$ GTP-CobW occurs proximal to (or in complex with) CobNST-HBAD, consistent with a requirement for a GAP protein that is proposed to have prevented *in vitro* transfer, but it must be present in engineered *E. coli* (encoded by an introduced gene or that normally functions with native *E. coli* GTPases) (Figure 3). In this way, GTP hydrolysis, and hence the formation of the  $\text{Co}^{\text{II}}$ -complexes at high free energy, can be solely restricted to clients associated with a GAP. The unfavorable free energy gradient for  $\text{Co}^{\text{II}}$  transfer from intracellular exchangeable available  $\text{Co}^{\text{II}}$  to CobNST-HBAD is calculated to be overcome by the hydrolysis of GTP mediated by CobW.

The metallochaperone-mediated transfer of  $\text{Cu}^{\text{I}}$  from hypothetical exchangeable buffer molecules to destinations (superoxide dismutase, cytochrome oxidase, and  $\text{P}_1$ -type ATPases to the trans-Golgi network and metallothionein) follows favorable thermodynamic gradients for metal binding.<sup>24</sup> This appears analogous to the CbiK-mediated transfer of  $\text{Co}^{\text{II}}$  from exchangeable buffering molecules to SHC in idealized *Salmonella*, albeit promoted by the formation of the CbiK-SHC adduct as evidenced by comparing the  $K_m$  with the  $K_D$  for  $\text{Co}^{\text{II}}$  of CbiK alone (Figures 4 and 6). Notably, the free energy for complex formation by exchangeable buffered  $\text{Co}^{\text{II}}$  is substantially lower in *Salmonella* grown in standard LB media than in idealized cells (Figure 5), estimating less than 1%  $\text{Co}^{\text{II}}$  occupancy for CbiK alone but still enabling 12% occupancy of the CbiK-SHC adduct, which may be suited to sustaining catalytic CbiK activity (Table S2). In the metallochaperone-dependent pathway, considering  $\text{Co}^{\text{II}}$  alone, 79%  $\text{Co}^{\text{II}}$  occupancy of  $\text{Mg}^{\text{II}}$ GTP-CobW would be estimated in *Salmonella* grown in standard LB media (Figure 5 and Table S2), suggesting that the CobW metallochaperone may enable  $\text{Co}^{\text{II}}$  acquisition for  $\text{B}_{12}$  synthesis in organisms (including *Rhodobacter*) in which the free energy for available  $\text{Co}^{\text{II}}$  might be lower than that modeled for an idealized *Salmonella* cell. Unlike the metallochaperone-mediated delivery of  $\text{Cu}^{\text{I}}$ , the CobW-dependent delivery of  $\text{Co}^{\text{II}}$  does not simply follow a favorable thermodynamic gradient for metal binding, reflecting the requirement for energetic input from nucleotide cofactors. The atypical thermodynamic pathway in Figure 6 distinguishes

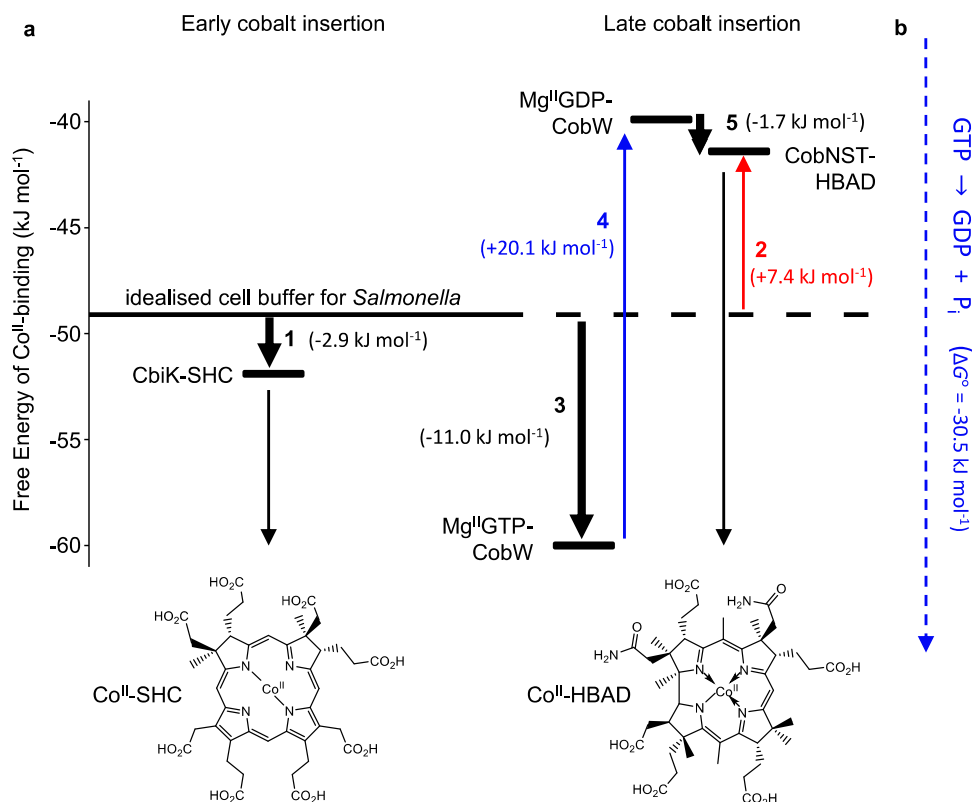


**Figure 6.** GTP-dependent CobW metallochaperone elevates the available free energy of Co<sup>II</sup> binding. (a) Free energies of Co<sup>II</sup>-complex formation in the CbiK versus CobW/CobNST pathways (free energy calculations in Table S4). Bold arrows denote Co<sup>II</sup> transfer. In the early cobalt insertion pathway, binding of the substrate SHC provides sufficient thermodynamic driving force for the chelatase CbiK to acquire Co<sup>II</sup> from the intracellular milieu of idealized *Salmonella* without the need of an additional chaperone (1). Conversely, in the late cobalt insertion pathway, Co<sup>II</sup> transfer from the intracellular milieu to the substrate bound chelatase, CobNST-HBAD, is thermodynamically unfavorable (2, red). Binding of Mg<sup>II</sup>GTP provides the necessary free energy gradient for the chaperone CobW to acquire Co<sup>II</sup> in a cell (3) and nucleotide hydrolysis to generate Mg<sup>II</sup>GDP-CobW (4, blue) elevates the free energy of Co<sup>II</sup> binding sufficiently to enable Co<sup>II</sup> transfer to CobNST-HBAD (5). Representations of Co<sup>II</sup>-SHC and Co<sup>II</sup>-HBAD are placed below the scale reflective of undetermined free energy values. (b) Magnitude of the standard free energy for hydrolysis of GTP (dashed blue) is shown for comparison (note common scales but arbitrary placement of y-axis in panel (b)).

the CobW-dependent pathway from the Cu<sup>I</sup> metallochaperone and the CbiK-dependent pathways. This also highlights metallochaperones as a mechanistically and perhaps functionally diverse grouping of proteins.

Affinities for multiple metals, coupled with intracellular availabilities revealed that Mg<sup>II</sup>GTP-CobW is vulnerable to mismetalation with Zn<sup>II</sup> when expressed in *E. coli*.<sup>4</sup> Here, we calculate that Zn<sup>II</sup> mismetalation of Mg<sup>II</sup>GTP-CobW would also be liable to occur in *Salmonella* grown in LB media (Table S5), raising questions about the relative availabilities of these two metals in the native (CobW-containing) Rhodobacter. Potentially, rates of GTP hydrolysis might be higher with Co<sup>II</sup> bound rather than Zn<sup>II</sup>, helping to avoid any incorrect metal transfer from CobW. CbiK was previously seen to be most likely to be mismetalated by Fe<sup>II</sup>, albeit only 1% Fe<sup>II</sup> occupancy was estimated in idealized *Salmonella* (ref<sup>14</sup> and Table S5). Whether or not there would be greater Fe<sup>II</sup> binding at the lesser Co<sup>II</sup> availability in *Salmonella* cells grown in LB media compared to idealized cells would depend upon the K<sub>m</sub> for Fe<sup>II</sup> insertion by SHC-CbiK and the extent to which Fe<sup>II</sup> availability also departs from idealized cells. Cobalt supplementation does also correlate with an increase in the total number of cobalt atoms per cell and decreases in the total number of atoms of iron (nickel and zinc) per cell (Figure S8). Notably, CbiK can also contribute to the synthesis of siroheme

sufficient to partly complement cells missing the siroheme ferrochelatase CysG.<sup>17</sup>

Our findings suggest that it would be fruitful to explore whether or not other GTP-dependent metallochaperones enable the transfer of their cognate metals against unfavorable thermodynamic gradients. A client for the GE3 GTPase Zng1 has recently been identified as Zn<sup>II</sup>-requiring methionine aminopeptidase I.<sup>25,26</sup> Deletion of ZNG1 in *Saccharomyces cerevisiae* impairs Map1 activity which in turn inhibits growth under Zn<sup>II</sup>-deficient conditions.<sup>25</sup> Similarly, zebrafish and mouse mutants in Zng1 show increased sensitivity to dietary Zn<sup>II</sup> starvation.<sup>26</sup> It has been suggested that Map1 may in effect be unable to compete with exchangeable labile Zn<sup>II</sup> buffer sites during Zn<sup>II</sup> limitation and the assistance of Zng1 prioritizes the metalation of Map1 under these conditions.<sup>25</sup> Bacterial cells also prioritize metalation of critical Zn<sup>II</sup> clients under Zn<sup>II</sup> limitation by sparing Zn<sup>II</sup> demand from ribosomal subunits,<sup>27–29</sup> modeled to occur when the degree of buffer saturation equates to a 100-fold decrease in available [Zn<sup>II</sup>] (Figure 4b from Osman and co-workers<sup>14</sup>). This equates to a change in free energy for metal complex formation of -11.4 kJ mol<sup>-1</sup>. Figure 6 shows that hydrolysis of Co<sup>II</sup>Mg<sup>II</sup>GTP-CobW elevates the free energy of Co<sup>II</sup> binding by 20 kJ mol<sup>-1</sup>. It is plausible that Zng1 similarly acts to overcome an unfavorable thermodynamic gradient for Zn<sup>II</sup> transfer from the intracellular milieu to Map1 when Zn<sup>II</sup> becomes limiting. Notably, CobW



still enhanced B<sub>12</sub> production in 300  $\mu$ M Co<sup>II</sup> where CobNST is estimated to be substantially independently metalated, raising the tantalizing possibility that the metallochaperone also enhances  $k_{\text{cat}}$  for the enzymatic reaction in addition to overcoming an unfavorable thermodynamic gradient for Co<sup>II</sup> transfer.

## CONCLUSIONS

The present work has revealed that the two pathways for vitamin B<sub>12</sub> biosynthesis follow distinct thermodynamic gradients for the acquisition of Co<sup>II</sup> from the intracellular milieu. While Co<sup>II</sup> flows down a favorable gradient to CbiK-SHC, the G3E GTPase Mg<sup>II</sup>GTP-CobW can overcome an unfavorable gradient to CobNST-HBAD. Future studies should explore the intriguing implication that mechanisms exist to somehow shield hyper-available metal (at elevated  $\Delta G$ ) from solvent or nonspecific ligands to enable exclusive, tunneled/channeled transfer from GTP-dependent metallochaperones to their clients.

## METHODS

### Preparation of Metal and Ligand Stock Solutions

Metal stocks (CoCl<sub>2</sub>, MgCl<sub>2</sub> and ZnSO<sub>4</sub>) were prepared in ultrapure water in acid-washed glassware or clean plasticware to avoid metal contamination, with concentrations quantified by ICP-MS analysis. Ligands (NTA, EGTA, His) were prepared in ultrapure water from salts and adjusted to pH  $\sim$ 7.0 prior to use in assays where necessary (i.e., when [ligand] was sufficient to affect pH of assay solution). Metal and ligand stocks were filter-sterilized before addition to bacterial cultures.

### Protein Expression and Purification

The coding regions of *R. capsulatus cobN* were cloned into a pET14b vector with a 6 $\times$ His-tag and thrombin cleavage site-encoded N-terminal to the *cobN* sequence (see Figure S9 for sequence details). The coding regions of *R. capsulatus cobS* and *cobT* genes were cloned into a pET3a vector with two ribosome binding sites encoded, one immediately preceding each gene, for coexpression of the two gene products. The 6 $\times$ His-tag and thrombin cleavage site included N-terminal to *cobS* only (see Figure S10 for sequence details). *E. coli* BL21(DE3) pLysS transformed with either pET14b-*cobN* or pET3a-*cobST* was cultured (with shaking) at 37  $^{\circ}$ C in LB medium with antibiotics carbenicillin (100 mg L<sup>-1</sup>) and chloramphenicol (34 mg L<sup>-1</sup>). At mid-log phase, protein expression was induced by the addition of IPTG (0.4 mM) and cells were cultured (with shaking) at 20  $^{\circ}$ C overnight. Cells were harvested and stored at  $-20$   $^{\circ}$ C prior to use.

Cells overexpressing CobN or CobST were resuspended in 20 mM sodium phosphate pH 7.4, 500 mM NaCl, 5 mM imidazole, 5 mM DTT for lysis (sonication), and cell debris was pelleted by centrifugation (38,000g, 45 min, 4  $^{\circ}$ C). Lysate was loaded to a 5 mL HisTrap HP column (GE Healthcare) pre-equilibrated in suspension buffer. CobN and CobS bind to the column courtesy of the 6 $\times$ His-tags at the N-terminus of each peptide, and CobT (expressed without a His-tag) remains associated with CobS throughout purification. The column was washed with suspension buffer containing 50 mM imidazole and then eluted with suspension buffer containing 300 mM imidazole. Protein-containing fractions were incubated with excess EDTA (10 mM) for  $\geq$ 1 h before loading to a HiPrep 16/60 Sephacryl S-300 HR size exclusion column (Cytiva) equilibrated in chelex-treated buffer (20 mM Hepes pH 7.0, 150 mM NaCl, 5 mM DTT) and eluted in the same buffer. Peak protein-containing fractions (assessed by SDS-PAGE) were pooled, concentrated (to 0.5–1.0 mL) using a Vivaspin 15 Turbo centrifugal concentrator, and then moved to an anaerobic chamber. Concentrated samples were applied to a PD-10 desalting column prepacked with Sephadex G-25 medium (GE Healthcare) equilibrated with

chelex-treated and N<sub>2</sub>-purged buffer (20 mM HEPES pH 7.0, 100 mM NaCl) and eluted in the same buffer. Protein purity was confirmed by SDS-PAGE (Figures 1 and S1) and concentration quantified by A<sub>280 nm</sub> using extinction coefficients ( $\epsilon$  = 134,000 M<sup>-1</sup> cm<sup>-1</sup> for CobN and 92,000 M<sup>-1</sup> cm<sup>-1</sup> for CobST) predicted from bioinformatic analysis.

Expression and isolation of *R. capsulatus* CobW and *Salmonella* CbiK followed previously reported protocols.<sup>4,14</sup>

### Isolation of Sirohydrochlorin

Sirohydrochlorin (SHC) synthesis and isolation followed protocols described in refs 18, 30. *E. coli* BL21(DE3)pLysS transformed with pETcoco-2ABCD (encoding enzymes for SHC synthesis, see refs 18, 30) was cultured (with shaking) at 37  $^{\circ}$ C in LB medium with 0.2% (w/v) glucose, carbenicillin (100 mg L<sup>-1</sup>), and chloramphenicol (34 mg L<sup>-1</sup>). At mid-log phase (OD<sub>600 nm</sub>  $\sim$ 0.5), 0.02% (w/v) L-arabinose was added and cells cultured a further 2 h at 37  $^{\circ}$ C; then, protein expression was induced with IPTG (0.4 mM), and cells were cultured at 24  $^{\circ}$ C overnight before harvesting pellets. Cells were resuspended in 30 mM sodium phosphate pH 7.4, 100 mM NaCl, 5 mM imidazole for lysis (sonication), and cell debris was pelleted by centrifugation (38,000g, 45 min, 4  $^{\circ}$ C). Lysate was loaded to a 5 mL HisTrap HP column (GE Healthcare) pre-equilibrated in suspension buffer. The column was washed with suspension buffer containing 50 mM imidazole then eluted with suspension buffer containing 300 mM imidazole. The remaining procedure was conducted in an anaerobic chamber. Peak elution fractions ( $\sim$ 2.5 mL) were buffer-exchanged into N<sub>2</sub>-purged 50 mM Tris pH 8.5, 100 mM NaCl using a Sephadex G-25 gel-filtration column, then added to solution A, and left overnight in a foil-wrapped (to exclude light) glass vessel. Solution A contained 20 mg of S-adenosyl-L-methionine, 10 mg of aminolevulinic acid, and 6.5 mg of NAD dissolved in 2 mL of N<sub>2</sub>-purged 50 mM Tris and 100 mM NaCl and adjusted to pH 8.5 using NaOH. The reaction product was applied to a 1 mL HiTrap DEAE (diethylaminoethyl) FF (GE Healthcare) pre-equilibrated in N<sub>2</sub>-purged reaction buffer and washed with the same buffer containing 100, 200, and 300 mM NaCl (5 mL each); then, SHC was eluted in the same buffer containing 1 M NaCl. SHC was stored frozen at  $-80$   $^{\circ}$ C in airtight tubes and concentration quantified using  $\epsilon_{376 \text{ nm}}$  = 240,000 M<sup>-1</sup> cm<sup>-1</sup> ref 22.

### Isolation of Hydrogenobyrrinic Acid $\alpha,\epsilon$ -Diamide

Hydrogenobyrrinic acid  $\alpha,\epsilon$ -diamide (HBAD) synthesis and isolation followed protocols described in ref 19, using *E. coli* strain ED549, engineered with genes for biosynthesis of hydrogenobyrrinic acid from the endogenous *E. coli* precursor uroporphyrinogen III. *E. coli* strain ED549 is BL21 star(DE3)(pLysS-DNAJ<sup>RC</sup>-ORF647<sup>RC</sup>) (pETcoco2-*cobA*<sup>Mbar</sup>-*cobIG*<sup>Bmei</sup>-*cobJFMKLH*<sup>RC</sup>(B)<sup>Bmei</sup>) where RC denotes *R. capsulatus*, Mbar denotes *M. barkeri*, and Bmei denotes *Brucella melitensis*. 1L media (10 g yeast extract, 16 g tryptone, 5 g NaCl, 1 g NH<sub>4</sub>Cl) with ampicillin (100 mg/L) and chloramphenicol (34 mg/L) were inoculated with an overnight culture of ED549 and incubated at 28  $^{\circ}$ C with shaking (160 rpm) for 6 h before adding L-arabinose (0.2% (w/v)) and then continuing incubation at 28  $^{\circ}$ C with shaking (160 rpm) overnight. The resulting cell pellets, which contained a mixture of hydrogenobyrrinic acid (HBA) and HBAD, were resuspended in 10 mM Hepes buffer pH 7.5, sonicated, and centrifuged, and the supernatant boiled for 5 min and centrifuged. The supernatant was mixed with ATP (5 mM), MgCl<sub>2</sub> (20 mM), L-glutamine (5 mM), and crude extract of *E. coli* strain BL21 star(DE3)(pLysS-DNAJ<sup>RC</sup>-cobB<sup>RC</sup>) (pET3a-cobB<sup>Bmei</sup>), which contained overexpressed *R. capsulatus* CobB and *Brucella melitensis* CobB for conversion of HBA to HBAD, and the mixture was left in the dark at room temperature overnight. The resulting supernatant was applied to a DEAE column pre-equilibrated in buffer (20 mM Hepes pH 7.5, 100 mM NaCl) washed with buffer containing 100 mM NaCl and HBAD eluted in buffer containing 200 mM NaCl. HBAD fractions were pooled and pH was adjusted to 4 using 1 M HCl before applying to an RP18 resin (preactivated in methanol and then rinsed with H<sub>2</sub>O + 0.1% TFA before applying the HBAD sample). The resin was washed with H<sub>2</sub>O + 0.1% TFA and then with 10% methanol, and HBAD eluted with 50% methanol. Solutions were freeze-dried and



stored in the dark at  $-20\text{ }^{\circ}\text{C}$ . HBAD was resolubilized in  $\text{H}_2\text{O}$  as required and quantified using a reported extinction coefficient at  $\lambda_{\text{max}} \sim 325\text{ nm}$  of  $\epsilon = 50,000\text{ cm}^{-1}\text{ M}^{-1}$  ref 9.

### Steady-State Enzyme Kinetic Assays

Reactions were prepared in an anaerobic chamber using chelex-treated,  $\text{N}_2$ -purged 50 mM Hepes buffer pH 7.0, 100 mM NaCl and monitored spectroscopically using a sealed 1 cm path length quartz cuvette at room temperature ( $20\text{--}25\text{ }^{\circ}\text{C}$ ).

For CobNST enzyme assays, absorbance of the tetrapyrrole substrate HBAD in a quartz cuvette with 1.0 cm path length was monitored by continuous cycling ( $200\text{--}800\text{ nm}$ ) using a Lambda 35 UV–visible spectrophotometer (PerkinElmer). Concentrations of the metalated product, cobyrinic acid  $\alpha,\text{c}$ -diamide (CBAD), were quantified from changes in the absorbance of 330 nm, using  $\Delta\epsilon_{330\text{ nm}} = -30,000\text{ M}^{-1}\text{ cm}^{-1}$  determined for cobalt chelation (Figures 2a and S2). The rates of metalation ( $v_0$ ) of HBAD were calculated from linear fits to changes in  $[\text{Co}^{\text{II}}\text{-HBAD}]$  over the first 6 min of reactions (as shown in Figure 2c). All reactions contained  $[\text{HBAD}] = 10\text{ }\mu\text{M}$ ,  $[\text{Co}^{\text{II}}]_{\text{tot}} = 100\text{ }\mu\text{M}$ ,  $[\text{Mg}^{\text{II}}] = 10\text{ mM}$ ,  $[\text{ATP}] = 5\text{ mM}$  (adjusted to pH 7.0 and quantified using  $\epsilon_{260\text{ nm}} = 1.54 \times 10^4\text{ M}^{-1}\text{ cm}^{-1}$ ), and  $[\text{CobN}] = [\text{CobST}] = 3.0\text{ }\mu\text{M}$  (based on monomeric concentrations of each subunit). Six subunits each of CobS and CobT appear to assemble a two-tiered hexameric ring, which likely docks with a single subunit of CobN to form the cobaltochelatase;<sup>5,10</sup> hence, the concentration of the active CobNST enzyme was estimated to be one-sixth of the total  $[\text{CobST}]_{\text{monomeric}}$  (CobN, present at equimolar concentrations to CobST, was in excess in the reaction mixture). The available  $\text{Co}^{\text{II}}$  concentration was adjusted using buffering ligands (L-His, EGTA) as listed in Table S1. Under the experimental conditions, with an excess of  $\text{Mg}^{\text{II}}$  over ATP, the effect of ATP on free  $\text{Co}^{\text{II}}$  concentrations, and hence, the estimated  $K_{\text{m}}$  value for CobNST, appears to be minimal (Calculation S2). Reactions were performed in triplicate to produce a mean rate, calculated as moles of HBAD metalated per mol enzyme per min, for each available  $\text{Co}^{\text{II}}$  concentration (Table S1). The appearance of a feature at  $\sim 350\text{ nm}$  is indicative of some conversion of the product to the  $\text{Co}^{\text{III}}$ -form,<sup>9</sup> encouraging the subsequent replacement of the oxygen detector in the anaerobic chamber.

For CbiK enzyme assays, absorbance at 375 nm was monitored in a quartz cuvette with a 1.0 cm path length using a Multiscan GO spectrophotometer (Thermo Scientific). Concentrations of metalated sirohydrochlorin produced were quantified from changes in absorbance at 375 nm, using  $\Delta\epsilon_{375\text{ nm}} = -140,000\text{ M}^{-1}\text{ cm}^{-1}$  determined for cobalt chelation (Figures 4a and S2). The rates of metalation ( $v_0$ ) of SHC were calculated from linear fits to changes in  $[\text{Co}^{\text{II}}\text{-SHC}]$  over the first 2 min of reactions (as shown in Figure 4c). Reactions contained  $[\text{SHC}] = 5\text{ }\mu\text{M}$ ,  $[\text{Co}^{\text{II}}]_{\text{tot}} = 100\text{ }\mu\text{M}$ , and  $[\text{CbiK}] = 0.375\text{ }\mu\text{M}$ . Available  $\text{Co}^{\text{II}}$  concentrations were adjusted using buffering ligands (His, NTA, and EGTA) with high concentrations of histidine ( $[\text{His}]_{\text{tot}} > 1\text{ mM}$ ) avoided (see Figure S11). Ligands were added first to quench nonenzymatic metalation (see Figure 4b), and CbiK was added last to initiate the enzymatic reaction. Reactions were performed in triplicate to produce a mean rate, calculated as moles of SHC metalated per mol CbiK per min, for each available  $\text{Co}^{\text{II}}$  concentration (Table S3).

Steady-state kinetics data were fitted to eq 1

$$v_0/[\text{E}]_{\text{tot}} = \frac{k_{\text{cat}}[\text{Co}^{\text{II}}]}{[\text{Co}^{\text{II}}] + K_{\text{m}}} \quad (1)$$

using Microsoft Excel with fitted values for  $k_{\text{cat}}$  and  $K_{\text{m}}$  generated by minimizing the least-squares error across each dataset. This model assumes that enzymes were fully saturated with their tetrapyrrole substrates which were supplied in excess; thus, only the available  $[\text{Co}^{\text{II}}]$  (buffered using ligands, see Tables S1 and S3) was rate-limiting. The Michaelis constant ( $K_{\text{m}}$ ) is described by eq 2

$$K_{\text{m}} = \frac{k_{-1} + k_{\text{cat}}}{k_1} \quad (2)$$

where  $k_1$  and  $k_{-1}$  are the on and off rates, respectively, for  $\text{Co}^{\text{II}}$  binding to the enzyme–substrate complex and  $k_{\text{cat}}$  is the rate of  $\text{Co}^{\text{II}}$  insertion into the tetrapyrrole. When  $k_{-1} \gg k_{\text{cat}}$  (i.e., metal dissociation is significantly faster than the turnover number of the enzyme),  $K_{\text{m}}$  approximates the  $K_{\text{D}} \left( = \frac{k_{-1}}{k_1} \right)$  for  $\text{Co}^{\text{II}}$  binding. The

presence of a large amount of buffered metal (relative to enzyme and tetrapyrrole substrate concentrations) means that the total number of  $\text{Co}^{\text{II}}$  atoms in the buffer (and hence the available  $[\text{Co}^{\text{II}}]$ ) did not significantly change over the course of the experiment and adventitious  $\text{Co}^{\text{II}}$  binding at nonenzymatic sites (eg His-tags on CobNST) should have negligible impact on the measured  $K_{\text{m}}$ .

### Growth of Salmonella

All cultures and media were prepared in plasticware or acid-washed glassware to minimize trace metal contamination. For quantification of total metal, total corrin, and intracellular available  $\text{Co}^{\text{II}}$  concentrations in anaerobic  $\text{B}_{12}$ -producing *Salmonella*, LB medium was inoculated with overnight culture of *S. enterica* serovar Typhimurium strain 1344 ( $\text{OD}_{600\text{ nm}} = 0.025$ ) and incubated aerobically at  $37\text{ }^{\circ}\text{C}$  with shaking until  $\text{OD}_{600\text{ nm}}$  reached  $\sim 0.5$ . Aliquots (30 mL) of this culture were treated with  $\text{CoCl}_2$ ,  $\text{H}_2\text{O}$ , or EDTA (0.3 mL of  $100\times$  concentrated stocks) to reach final concentrations specified in figure legends and then incubated statically at  $37\text{ }^{\circ}\text{C}$  in an airtight container together with Oxoid AnaeroGen anaerobic gas-generating sachets (Thermo Fisher Scientific). After 3 h of anaerobic incubation,  $\text{OD}_{600\text{ nm}}$  of each culture (Figure S12a) were recorded using a Multiscan GO spectrophotometer (Thermo Scientific), and samples for RNA extraction, quantification of corrins, and quantification of metal were collected from each culture.

For quantification of intracellular available  $\text{Zn}^{\text{II}}$  concentrations in aerobic *Salmonella*, LB medium was inoculated with overnight culture of *S. enterica* serovar Typhimurium strain 1344 ( $\text{OD}_{600\text{ nm}} = 0.025$ ) and incubated aerobically at  $37\text{ }^{\circ}\text{C}$  with shaking until  $\text{OD}_{600\text{ nm}}$  reached  $\sim 0.3$ . Aliquots (2.5 mL) of this culture were treated with  $\text{ZnSO}_4$ ,  $\text{H}_2\text{O}$ , or TPEN (25  $\mu\text{L}$  of  $100\times$  concentrated stocks) to reach final concentrations specified in figure legends and then incubated at  $37\text{ }^{\circ}\text{C}$  for a further 1 h before collecting samples for RNA extraction and  $\text{OD}_{600\text{ nm}}$  (Figure S12b).

### Determination of Transcript Abundance in Salmonella

Samples (1 mL) of *Salmonella* cultures were stabilized in an RNAProtect Bacteria Reagent (2 mL; Qiagen) and cell pellets frozen at  $-80\text{ }^{\circ}\text{C}$  for up to 1 week prior to RNA extraction. RNA was extracted using an RNeasy Mini Kit (Qiagen) as described by the manufacturer. RNA was quantified by absorbance at 260 nm and then treated with DNase I (1 U/ $\mu\text{g}$  RNA; Fermentas) for 1 h at  $37\text{ }^{\circ}\text{C}$ . cDNA was generated using an ImProm-II Reverse Transcriptase System (Promega) with 300 ng of RNA per reaction, and control reactions without transcriptase were conducted in parallel. Transcript abundance was determined using primers 1 and 2 for *rcnA*, 3 and 4 for *rrsD*, 5 and 6 for *rpoD*, 7 and 8 for *znuA*, and 9 and 10 for *zntA* (Table S6). Quantitative PCR analysis was carried out in 20  $\mu\text{L}$  reactions using 5 ng of cDNA, 0.8  $\mu\text{M}$  of the appropriate primers, and Power Up SYBR Green Master Mix (Thermo Fisher Scientific). Three technical replicates of each sample (ie biological replicate) were analyzed using a Rotor-Gene Q 2plex (Qiagen; Rotor-Gene-Q Pure Detection software), plus control reactions without cDNA template for each primer pair. *rpoD* was used as the reference gene in analyses of *znuA* and *zntA* transcript abundance from aerobic *Salmonella* cultures. Initial analysis of transcripts from anaerobic cultures treated with 1 mM EDTA or 500  $\mu\text{M}$   $\text{Co}^{\text{II}}$  showed significant changes in *rpoD*  $C_{\text{q}}$  values (suggesting that *rpoD* expression may have been affected by the most extreme concentrations of chelator or  $\text{Co}^{\text{II}}$ ) but not in *rrsD*  $C_{\text{q}}$  values which remained consistent across all samples (Table S7); thus, *rrsD* was selected as the reference gene for analyses of *rcnA* transcript abundance in anaerobic *Salmonella*. The fold change in gene abundance, relative to the mean of the control condition (defined as the condition where minimum gene transcript abundance was observed), was calculated using the  $2^{-\Delta\Delta\text{CT}}$  method.<sup>31</sup>  $C_{\text{q}}$  values

were calculated with LinRegPCR (version 2016.1) after correcting for amplicon efficiency.<sup>32</sup>

### Intracellular Available $\Delta G_{\text{metal}}$ under Bespoke Conditions

Fractional responses ( $\theta_D$  or  $\theta_{DM}$ ) of *Salmonella* metal sensors were calculated as described by Foster and co-workers<sup>15</sup> using eq 3 for repressors (RcnR and Zur) and eq 4 for activators (ZntA)

$$\theta_D = 0.99 - 0.98 \times \left( \frac{\text{fold change}_{\text{obs}} - 1}{\text{fold change}_{\text{max}} - 1} \right) \quad (3)$$

$$\theta_{DM} = 0.01 + 0.98 \times \left( \frac{\text{fold change}_{\text{obs}} - 1}{\text{fold change}_{\text{max}} - 1} \right) \quad (4)$$

where fold change<sub>obs</sub> is the fold change in gene expression under the condition of interest and fold change<sub>max</sub> is the maximum observed fold change at the calibration limits (defined as corresponding to  $\theta_D$  or  $\theta_{DM}$  of 0.01 and 0.99, respectively). Fractional responses were converted to available intracellular metal concentrations using the excel spreadsheet (Supporting Dataset 1) and MATLAB code (Supporting Note 3) from Osman and co-workers,<sup>14</sup> together with known metal affinity, DNA affinities, and protein abundances determined for *Salmonella* sensors.<sup>14</sup>

Intracellular available  $\Delta G_{\text{metal}}$  was calculated using eq 5

$$\Delta G_{\text{metal}} = RT \ln [\text{metal}] \quad (5)$$

where [metal] is the intracellular available metal concentration,  $R$  (gas constant) =  $8.314 \times 10^{-3} \text{ kJ K}^{-1} \text{ mol}^{-1}$ , and  $T$  (temperature) = 298.15 K.

### Quantification of Total Metal and Vitamin B<sub>12</sub> in *Salmonella* Cultures

Samples (10 mL) of *Salmonella* cultures were pelleted, washed twice with wash buffer (0.5M sorbitol, 200  $\mu\text{M}$  EDTA, 20 mM Tris pH 8.5), and frozen at  $-20^\circ\text{C}$  prior to processing. The number of cells in each sample was estimated using a correlation factor previously determined for *E. coli* cells ( $4.4 \pm 0.1 \times 10^8 \text{ cells mL}^{-1} \text{ OD}_{600 \text{ nm}}^{-1}$ , ref 4) to convert  $\text{OD}_{600 \text{ nm}}$  to cell number. Cell pellets were resuspended in 200  $\mu\text{L}$  of  $\text{H}_2\text{O}$ , boiled for 15 min ( $100^\circ\text{C}$ ) and centrifuged to remove cell debris. Supernatants were analyzed for total corrin and total metal.

To quantify corrin production (assumed to be predominantly B<sub>12</sub> since *S. enterica* serovar Typhimurium strain 1344 contains genes for the complete pathway), an aliquot (5  $\mu\text{L}$ ) of each supernatant was applied to *Salmonella typhimurium* AR2680 ( $\Delta\text{metE}$ ,  $\Delta\text{cbiB}$ ) bioassay plates<sup>33</sup> and incubated at  $37^\circ\text{C}$  overnight. Plates were imaged on a black background GelDoc XR + gel documentation system (BioRad, ImageLab software), and diameters of growth were measured (blinded) from images. A calibration curve relating growth diameters to B<sub>12</sub> concentration was generated using B<sub>12</sub> standards (cyanocobalamin, 1–1000 nM, quantified by  $A_{360 \text{ nm}} = 27,500 \text{ M}^{-1} \text{ cm}^{-1}$  at pH 10, ref 34) in parallel with cell lysates, using the same batch of bioassay plates.

To quantify the total metal content, 100  $\mu\text{L}$  of each supernatant was diluted 40-fold in 2.5%  $\text{HNO}_3$  (total volume = 4 mL) before metal analysis by ICP-MS.

## ■ ASSOCIATED CONTENT

### SI Supporting Information

The Supporting Information is available free of charge at <https://pubs.acs.org/doi/10.1021/jacsau.3c00119>.

Additional experimental results and calculations including rates of metalation of hydrogenobyrinic acid a,c-diamide (HBAD) by CobNST at varying cobalt availabilities (Table S1); calculated  $\text{Co}^{\text{II}}$  occupancies of proteins (CobW, CobNST, and CbiK) in bacterial cells (Table S2); rates of metalation of sirohydrochlorin

(SHC) by CbiK at varying cobalt availabilities (Table S3); free energies for  $\text{Co}^{\text{II}}$  binding (Table S4); calculated  $\text{Co}^{\text{II}}$  occupancies of CobW and CbiK, taking into account competition from  $\text{Fe}^{\text{II}}$  and  $\text{Zn}^{\text{II}}$  (Table S5); oligonucleotides used in this work (Table S6); Cq values from qPCR analysis of reference genes (*rpoD* and *rrsD*) in *Salmonella* samples following 3 hr exposure to metal or a chelator under anaerobic conditions (Table S7); SDS-PAGE gels of proteins purified from *E. coli* (Figure S1); UV–visible absorbance of cobaltochelate substrates and products (Figure S2); rates of enzymatic  $\text{Co}^{\text{II}}$  insertion into tetrapyrrole substrates as a function of total enzyme concentration (Figure S3); CobNST-catalyzed metalation of HBAD with or without CobW in the presence of surplus total  $\text{Co}^{\text{II}}$  (Figure S4);  $\text{Mg}^{\text{II}}$ GTP-CobW binds and fully withholds  $\text{Co}^{\text{II}}$  from CobNST when total CobW is supplied in excess of total  $\text{Co}^{\text{II}}$  (Figure S5); quantification of vitamin B<sub>12</sub> in *Salmonella* cultures (Figure S6); intracellular  $\text{Zn}^{\text{II}}$  availability in *Salmonella* (Figure S7); total metal content of *Salmonella* cells (Figure S8); DNA sequence of the pET14b-CobN vector between BglII and BmtI restriction sites (including the coding region for CobN) (Figure S9); DNA sequence of the pET3a-CobST vector between BglII and SpeI restriction sites (including coding regions for CobS and CobT) (Figure S10); rates of metalation of SHC by CbiK with different  $\text{Co}^{\text{II}}$ -buffering ligands (Figure S11); optical density of *Salmonella* cultures (Figure S12); calculation of  $\text{Co}^{\text{II}}$  occupancies of CobW and CobNST in the metal transfer complex (Calculation S1); and calculations to assess the influence ATP on available [ $\text{Co}^{\text{II}}$ ] during CobNST enzymatic assays (Calculation S2) (PDF)

## ■ AUTHOR INFORMATION

### Corresponding Authors

Tessa R. Young – Department of Biosciences, Durham University, Durham DH1 3LE, U.K.; Department of Chemistry, Durham University, Durham DH1 3LE, U.K.; [orcid.org/0000-0002-7373-1969](https://orcid.org/0000-0002-7373-1969); Email: [tessa.r.young@durham.ac.uk](mailto:tessa.r.young@durham.ac.uk)

Nigel J. Robinson – Department of Biosciences, Durham University, Durham DH1 3LE, U.K.; Department of Chemistry, Durham University, Durham DH1 3LE, U.K.; Email: [nigel.robinson@durham.ac.uk](mailto:nigel.robinson@durham.ac.uk)

### Authors

Evelyn Deery – School of Biosciences, University of Kent, Canterbury CT2 7NJ, U.K.

Andrew W. Foster – Department of Biosciences, Durham University, Durham DH1 3LE, U.K.; Department of Chemistry, Durham University, Durham DH1 3LE, U.K.

Maria Alessandra Martini – Department of Biosciences, Durham University, Durham DH1 3LE, U.K.; Department of Inorganic Spectroscopy, Max Planck Institute for Chemical Energy Conversion, 45470 Mülheim an der Ruhr, Germany; [orcid.org/0000-0002-6558-206X](https://orcid.org/0000-0002-6558-206X)

Deenah Osman – Department of Biosciences, Durham University, Durham DH1 3LE, U.K.; Department of Chemistry, Durham University, Durham DH1 3LE, U.K.

Martin J. Warren – School of Biosciences, University of Kent, Canterbury CT2 7NJ, U.K.; Quadram Institute Bioscience, Norwich Research Park, Norwich NR4 7UQ, U.K.

Complete contact information is available at:  
<https://pubs.acs.org/10.1021/jacsau.3c00119>

### Author Contributions

T.R.Y. conducted *in vitro* assays and *in vivo* experiments for cobalt-treated *Salmonella* and *E. coli*. E.D. generated protein overexpression plasmids. E.D. and M.J.W. donated SHC- and HBAD-producing strains. E.D., M.J.W., and A.W.F. advised on purification protocols and biochemistry. M.A.M. determined zinc availabilities in *Salmonella*. D.O. performed ICP-MS analyses. T.R.Y. and N.J.R. wrote the manuscript with input from M.A.M., E.D., and M.J.W. T.R.Y. and N.J.R. interpreted the significance of the data and had overall responsibility for design and management of the project. All authors have given approval to the final version of the manuscript.

### Notes

The authors declare no competing financial interest.

### ACKNOWLEDGMENTS

This work was supported by a Royal Commission for the Exhibition of 1851 Research Fellowship (T.R.Y.), Royal Society Industrial Fellowship INF\R2\180062 (M.J.W.), and Biotechnology and Biological Sciences Research Council awards BB/V006002/1, BB/W015749/1, BB/S009787/1, BB/S002197/1, and BBS/E/F/000PR10346. The authors acknowledge the use of the Durham Biological ICP-MS facility (Durham University, U.K.) and thank members of the research group Arthur Glasfeld and Sophie Clough for constructive scientific discussions. The authors especially acknowledge the contributions of Deenah Morton (nee Osman) who passed away on 28th August 2022.

### ABBREVIATIONS

ATP	adenosine triphosphate
CBAD	cobyrinic acid <i>a,c</i> -diamide
EDTA	ethylenediaminetetraacetic acid
EGTA	ethyleneglycol-bis( $\beta$ -aminoether)- <i>N,N',N',N'</i> -tetraacetic acid
GAP	GTPase-activating protein
GTP	guanosine triphosphate
HBAD	hydrogenobyrinic acid <i>a,c</i> -diamide
His	histidine
LB	Luria-Bertani
SDS-PAGE	sodium dodecyl sulfate polyacrylamide gel electrophoresis
SHC	sirohydrochlorin
qPCR	quantitative polymerase chain reaction

### REFERENCES

- (1) Foster, A. W.; Osman, D.; Robinson, N. J. Metal preferences and metallation. *J. Biol. Chem.* **2014**, *289*, 28095–28103.
- (2) Bryant, D. A.; Hunter, C. N.; Warren, M. J. Biosynthesis of the modified tetrapyrroles: The pigments of life. *J. Biol. Chem.* **2020**, *295*, 6888–6925.
- (3) Foster, A. W.; Young, T. R.; Chivers, P. T.; Robinson, N. J. Protein metallation in biology. *Curr. Opin. Chem. Biol.* **2022**, *66*, No. 102095.
- (4) Young, T. R.; Martini, M. A.; Foster, A. W.; Glasfeld, A.; Osman, D.; Morton, R. J.; Deery, E.; Warren, M. J.; Robinson, N. J.

Calculating metallation in cells reveals CobW acquires Co<sup>II</sup> for vitamin B<sub>12</sub> biosynthesis while related proteins prefer Zn<sup>II</sup>. *Nat. Commun.* **2021**, *12*, 1195.

(5) Osman, D.; Cooke, A.; Young, T. R.; Deery, E.; Robinson, N. J.; Warren, M. J. The requirement for cobalt in vitamin B<sub>12</sub>: A paradigm for protein metallation. *Biochim. Biophys. Acta Mol. Cell Res.* **2021**, *1868*, No. 118896.

(6) Moore, Simon J.; Warren, Martin J. The anaerobic biosynthesis of vitamin B<sub>12</sub>. *Biochem. Soc. Trans.* **2012**, *40*, 581–586.

(7) Brindley, A. A.; Raux, E.; Leech, H. K.; Schubert, H. L.; Warren, M. J. A story of chelatase evolution: Identification and characterisation of a small 13–15kDa “ancestral” cobaltochelatase (CbiXS) in the archaea. *J. Biol. Chem.* **2003**, *278*, 22388–22395.

(8) Reid, J. D.; Hunter, C. N. Current understanding of the function of magnesium chelatase. *Biochem. Soc. Trans.* **2002**, *30*, 643–645.

(9) Debussche, L.; Couder, M.; Thibaut, D.; Cameron, B.; Crouzet, J.; Blanche, F. Assay, purification, and characterization of cobaltochelatase, a unique complex enzyme catalyzing cobalt insertion in hydrogenobyrinic acid *a,c*-diamide during coenzyme B<sub>12</sub> biosynthesis in *Pseudomonas denitrificans*. *J. Bacteriol.* **1992**, *174*, 7445–7451.

(10) Lundqvist, J.; Elmlund, D.; Heldt, D.; Deery, E.; Söderberg, C. A. G.; Hansson, M.; Warren, M.; Al-Karadaghi, S. The AAA<sup>+</sup> motor complex of subunits CobS and CobT of cobaltochelatase visualized by single particle electron microscopy. *J. Struct. Biol.* **2009**, *167*, 227–234.

(11) Woodward, R. B. The total synthesis of vitamin B<sub>12</sub>. *Pure Appl. Chem.* **1973**, *33*, 145–178.

(12) Eschenmoser, A.; Wintner, C. E. Natural product synthesis and vitamin B<sub>12</sub>: Total synthesis of vitamin B<sub>12</sub> provided a framework for exploration in several areas of organic chemistry. *Science* **1977**, *196*, 1410–1420.

(13) Moore, S. J.; Sowa, S. T.; Schuchardt, C.; Deery, E.; Lawrence, A. D.; Ramos, J. V.; Billig, S.; Birkemeyer, C.; Chivers, P. T.; Howard, M. J.; Rigby, S. E. J.; Layer, G.; Warren, M. J. Elucidation of the biosynthesis of the methane catalyst coenzyme F<sub>430</sub>. *Nature* **2017**, *543*, 78–82.

(14) Osman, D.; Martini, M. A.; Foster, A. W.; Chen, J.; Scott, A. J. P.; Morton, R. J.; Steed, J. W.; Lurie-Luke, E.; Huggins, T. G.; Lawrence, A. D.; Deery, E.; Warren, M. J.; Chivers, P. T.; Robinson, N. J. Bacterial sensors define intracellular free energies for correct enzyme metallation. *Nat. Chem. Biol.* **2019**, *15*, 241–249.

(15) Foster, A. W.; Clough, S. E.; Aki, Z.; Young, T. R.; Clarke, A. R.; Robinson, N. J. Metallation calculators for *E. coli* strain JM109 (DE3): Aerobic, anaerobic and hydrogen peroxide exposed cells cultured in LB media. *Metallomics* **2022**, No. mfac058.

(16) Fujishiro, T.; Ogawa, S. The nickel-sirohydrochlorin formation mechanism of the ancestral class II chelatase CfbA in coenzyme F<sub>430</sub> biosynthesis. *Chem. Sci.* **2021**, *12*, 2172–2180.

(17) Raux, E.; Thermes, C.; Heathcote, P.; Rambach, A.; Warren, M. J. A role for *Salmonella typhimurium* *cbiK* in cobalamin (vitamin B<sub>12</sub>) and siroheme biosynthesis. *J. Bacteriol.* **1997**, *179*, 3202–3212.

(18) Frank, S.; Deery, E.; Brindley, A. A.; Leech, H. K.; Lawrence, A.; Heathcote, P.; Schubert, H. L.; Brocklehurst, K.; Rigby, S. E. J.; Warren, M. J.; Pickersgill, R. W. Elucidation of Substrate Specificity in the Cobalamin (Vitamin B<sub>12</sub>) Biosynthetic Methyltransferases: Structure and Function of the C20 Methyltransferase (CbiL) from *Methanobacter Thermoautotrophicus*. *J. Biol. Chem.* **2007**, *282*, 23957–23969.

(19) Widner, F. J.; Lawrence, A. D.; Deery, E.; Heldt, D.; Frank, S.; Gruber, K.; Wurst, K.; Warren, M. J.; Kräutler, B. Total Synthesis, Structure, and Biological Activity of Adenosylrhodibalamine, the Non-Natural Rhodium Homologue of Coenzyme B<sub>12</sub>. *Angew. Chem., Int. Ed.* **2016**, *55*, 11281–11286.

(20) Heldt, D.; Lawrence, A.; Lindenmeyer, M.; Deery, E.; Heathcote, P.; Rigby, S.; Warren, M. Aerobic synthesis of vitamin B<sub>12</sub>: ring contraction and cobalt chelation. *Biochem. Soc. Trans.* **2005**, *33*, 815–819.



- (21) Reid, J. D.; Hunter, C. N. Magnesium-dependent ATPase Activity and Cooperativity of Magnesium Chelatase from *Synechocystis* sp. PCC6803. *J. Biol. Chem.* **2004**, *279*, 26893–26899.
- (22) Schubert, H. L.; Raux, E.; Brindley, A. A.; Leech, H. K.; Wilson, K. S.; Hill, C. P.; Warren, M. J. The structure of *Saccharomyces cerevisiae* Met8p, a bifunctional dehydrogenase and ferrochelatase. *EMBO J.* **2002**, *21*, 2068–2075.
- (23) Rodionov, D. A.; Hebbeln, P.; Gelfand, M. S.; Eitinger, T. Comparative and functional genomic analysis of prokaryotic nickel and cobalt uptake transporters: evidence for a novel group of ATP-binding cassette transporters. *J. Bacteriol.* **2006**, *188*, 317–327.
- (24) Banci, L.; Bertini, I.; Ciofi-Baffoni, S.; Kozyreva, T.; Zovo, K.; Palumaa, P. Affinity gradients drive copper to cellular destinations. *Nature* **2010**, *465*, 645–648.
- (25) Pasquini, M.; Grosjean, N.; Hixson, K. K.; Nicora, C. D.; Yee, E. F.; Lipton, M.; Blaby, I. K.; Haley, J. D.; Blaby-Haas, C. E. Zng1 is a GTP-dependent zinc transferase needed for activation of methionine aminopeptidase. *Cell Rep.* **2022**, *39*, No. 110834.
- (26) Weiss, A.; Murdoch, C. C.; Edmonds, K. A.; Jordan, M. R.; Monteith, A. J.; Perera, Y. R.; Rodríguez Nassif, A. M.; Petoletti, A. M.; Beavers, W. N.; Munneke, M. J.; Drury, S. L.; Krystofiak, E. S.; Thalluri, K.; Wu, H.; Kruse, A. R. S.; DiMarchi, R. D.; Caprioli, R. M.; Spraggins, J. M.; Chazin, W. J.; Giedroc, D. P.; Skaar, E. P. Zn-regulated GTPase metalloprotein activator 1 modulates vertebrate zinc homeostasis. *Cell* **2022**, *185*, 2148–2163.e2127.
- (27) Shin, J.-H.; Helmann, J. D. Molecular logic of the Zur-regulated zinc deprivation response in *Bacillus subtilis*. *Nat. Commun.* **2016**, *7*, 12612.
- (28) Ma, Z.; Gabriel, S. E.; Helmann, J. D. Sequential binding and sensing of Zn(II) by *Bacillus subtilis* Zur. *Nucleic Acids Res.* **2011**, *39*, 9130–9138.
- (29) Gilston, B. A.; Wang, S.; Marcus, M. D.; Canalizo-Hernández, M. A.; Swindell, E. P.; Xue, Y.; Mondragón, A.; O'Halloran, T. V. Structural and Mechanistic Basis of Zinc Regulation Across the *E. coli* Zur Regulon. *PLoS Biol.* **2014**, *12*, No. e1001987.
- (30) Lobo, S. A. L.; Brindley, A. A.; Romão, C. V.; Leech, H. K.; Warren, M. J.; Saraiva, L. M. Two Distinct Roles for Two Functional Cobaltochelatases (CbiK) in *Desulfovibrio vulgaris* Hildenborough. *Biochemistry* **2008**, *47*, 5851–5857.
- (31) Livak, K. J.; Schmittgen, T. D. Analysis of Relative Gene Expression Data Using Real-Time Quantitative PCR and the  $2^{-\Delta\Delta CT}$  Method. *Methods* **2001**, *25*, 402–408.
- (32) Ramakers, C.; Ruijter, J. M.; Deprez, R. H. L.; Moorman, A. F. M. Assumption-free analysis of quantitative real-time polymerase chain reaction (PCR) data. *Neurosci. Lett.* **2003**, *339*, 62–66.
- (33) Raux, E.; Lanois, A.; Levillayer, F.; Warren, M. J.; Brody, E.; Rambach, A.; Thermes, C. *Salmonella typhimurium* cobalamin (vitamin B<sub>12</sub>) biosynthetic genes: functional studies in *S. typhimurium* and *Escherichia coli*. *J. Bacteriol.* **1996**, *178*, 753–767.
- (34) Hill, J.; Pratt, J.; Williams, R. 987. The chemistry of vitamin B 12. Part I. The valency and spectrum of the coenzyme. *J. Chem. Soc. (Resumed)* **1964**, 5149–5153.